Available online at www.sciencedirect.com
SCIENCE DIRECT®
ELSEVIER
Journal of Magnetism and Magnetic Materials 293 (2005) 455–463
Journal of magnetism and magnetic materials
www.elsevier.com/locate/jmmm

Mathematical modelling of magnetically targeted drug delivery

Andrew D. Grief, Giles Richardson*

Theoretical Mechanics, School of Mathematical Sciences, University of Nottingham, University Park, Nottingham NG7 2RD, UK

Available online 3 March 2005

Abstract

A mathematical model for targeted drug delivery using magnetic particles is developed. This includes a diffusive flux of particles arising from interactions between erythrocytes in the microcirculation. The model is used to track particles in a vessel network. Magnetic field design is discussed and we show that it is impossible to specifically target internal regions using an externally applied field.
© 2005 Elsevier B.V. All rights reserved.

Keywords: Magnetic targeting; Drug delivery; Shear-induced diffusion; Network model; Magnetic field design; Simulation

1. Introduction

In conventional (systemic) drug delivery the drug is administered by intravenous injection; it then travels to the heart from where it is pumped to all regions of the body. Where the drug is aimed at a small target region this method is extremely inefficient and leads to much larger doses (often of toxic drugs) being used than necessary. In order to overcome this problem a number of targeted drug delivery methods have been developed. One of these, magnetically targeted drug delivery, involves binding a drug to small biocompatible magnetic particles (diameters $<5\times10^{-6}$ m), injecting these into the blood stream and using a high gradient magnetic field to pull them out of suspension in the target region. Once on the vessel wall the drug can either be released directly into the blood stream or a biological technique can be used to ensure uptake of the particles into the tissue. Recently there have been a number of promising animal [1] and clinical trials [2]. In this work we describe a theoretical analysis of this drug delivery technique.

Previous theoretical studies of magnetically targeted drug delivery have considered tracking individual particles under the influence of Stokes drag and a magnetic force alone [3,4]. Here we also consider interactions and collisions between moving red blood cells in the bloodstream which cause a diffusive motion of the magnetic particles much greater than the standard Brownian diffusion. We formulate a two-dimensional (2-D) model, suitable for studying the deposition of magnetic particles

*Corresponding author. Tel.: +44 115 95 13849; fax: +44 115 95 13837.
E-mail addresses: andrew.grief@nottingham.ac.uk (A.D. Grief), giles.richardson@nottingham.ac.uk (G. Richardson).

0304-8853/$ - see front matter © 2005 Elsevier B.V. All rights reserved.
doi:10.1016/j.jmmm.2005.02.040

within a network of blood vessels, in the limit of low diffusivity. Finally, we show (in two-dimensions) that it is impossible to target internal regions of the body using an externally applied magnetic field without targeting some surrounding regions more strongly. This leads us to speculate that magnetically targeted drug delivery is only suitable for target sites close to the edge of the body.

2. An advection–diffusion model

The motion of magnetic particles in the blood stream is modelled as an advection–diffusion process for the particle concentration $c(\boldsymbol{x},t)$. The particle velocity $\mathbf{v}_p$ in the blood stream is found by balancing hydrodynamic and magnetic forces. For a particle with hydrodynamic radius a in a fluid flow, velocity $\mathbf{v}_b$, Stokes drag law gives

$$\mathbf{v}_p = \mathbf{v}_b + \mathbf{v}_{mag}, \quad \text{where} \quad \mathbf{v}_{mag} = \frac{\mathbf{F}_{mag}}{6\pi\mu a}, \tag{1}$$

where μ is the dynamic viscosity of the fluid, and $\mathbf{F}_{mag}$ is the magnetic force on the particle. The Stokes drag coefficient must be modified when the particle is of the order of a few particle diameters from a solid boundary [5].

For small particles, Brownian motion may also be significant. This can be accounted for by introducing a particle diffusivity using the Einstein relation,

$$D_{Br} = kT/(6\pi\mu a).$$

Here T is the absolute temperature (measured in Kelvin) and k is Boltzmann's constant. A second diffusive mechanism that influences the particle motion in vessels larger than capillaries is '*shear-induced diffusion*'. Blood is a highly concentrated suspension of red blood cells suspended in plasma and when sheared cell—cell collisions give rise to random motions with a diffusive character [6]. This in turn drives a diffusive motion of the plasma, causing plasma borne particles and solutes to experience *shear-induced diffusion*, as has been shown experimentally in Ref. [7]. Measurements of the shear-induced diffusion coefficient of the plasma borne particles are difficult to obtain, however the scaling

$$D_{sh} = K_{sh}(r_{RBC})^2\dot{\gamma}$$

is quite well established [6,8] (Table 1). Here r_{RBC} is the blood cell radius and $\dot{\gamma}$ is the local value of the fluid shear rate, defined in terms of the strain rate tensor e_{ij} by the formula

$$\dot{\gamma} = (2e_{ij}e_{ij})^{1/2} = \left(\frac{1}{2}\left(\frac{\partial u_i}{\partial x_j}+\frac{\partial u_j}{\partial x_i}\right)\left(\frac{\partial u_i}{\partial x_j}+\frac{\partial u_j}{\partial x_i}\right)\right)^{1/2},$$

where K_{sh} a dimensionless coefficient that depends on the blood cell concentration. Experimental estimates of K_{sh} for red blood cells at physiological haematocrits show a high degree of scatter, but a value of $K_{sh} \approx 5 \times 10^{-2}$ is representative [8]. Note that the shear augmented diffusion coefficient is independent of the particle dimensions, so that D_{sh} will take the same value for a 10 nm particle and 1 μm microsphere. Representative values of D_{sh} for a range of blood vessels are shown in Table 1. The overall diffusion coefficient is given by the sum of the Brownian diffusivity and the shear-induced diffusivity, leading to a diffusive flux

$$\mathbf{J}_{diff} = -D\nabla c, \quad \text{where} \quad D = K_{sh}(r_{RBC})^2\dot{\gamma} + \frac{kT}{6\pi\mu a}. \tag{2}$$

Table 1
Typical values of the properties of the main types of blood vessel

Vessel type	Diameter (m)	Length (m)	U_b (m s^{-1})	$\dot{\gamma}$ (s^{-1})	D_{sh} (m^2 s^{-1})
Artery	3×10^{-3}	1×10^{-1}	1×10^{-1}	6×10^{1}	6×10^{-11}
Arteriole	3×10^{-5}	7×10^{-4}	1×10^{-2}	6×10^{2}	6×10^{-10}
Capillary	7×10^{-6}	6×10^{-4}	7×10^{-4}	2×10^{2}	N/A
Venule	4×10^{-5}	8×10^{-4}	4×10^{-3}	2×10^{2}	1.6×10^{-10}
Vein	5×10^{-3}	1×10^{-1}	1×10^{-1}	4×10^{1}	3.5×10^{-11}

We chose $r_{RBC} = 4.2 \times 10^{-6}$ m, $K_{sh} = 5 \times 10^{-2}$ when calculating $D_{sh} = K_{sh}r_{RBC}^2\gamma$.

Combining the advective flux, $\mathbf{J}_{\text{advect}} = c\,\mathbf{v}_{\text{p}}$, and the diffusive flux contributions, and using conservation of mass, leads to an advection–diffusion equation for the particle concentration c [9],

$$\frac{\partial c}{\partial t} + \nabla \cdot (c\mathbf{v}_{\text{p}}) = \nabla \cdot (D\nabla c). \tag{3}$$

The model is closed (when $D<0$) by imposing boundary conditions on c. These can be derived by relating the flux of particles onto the boundary of the blood vessels to the evolution of the surface density of particles on the vessel wall, $\sigma(x,t)$,

$$\begin{aligned}\frac{\partial \sigma}{\partial t} &= \mathbf{n} \cdot [\mathbf{J}_{\text{advect}} + \mathbf{J}_{\text{diff}}]|_{\text{boundary}} \\ &= \mathbf{n} \cdot [c\mathbf{v}_{\text{mag}} - D\nabla c]|_{\text{boundary}},\end{aligned} \tag{4}$$

($\mathbf{n}$ is the outward unit normal vector at the boundary, $\mathbf{v}_{\text{b}} = \mathbf{0}$ at the boundary) and modelling the evolution of σ by taking the particle adhesion rate to be proportional to $c(\boldsymbol{x},t)$ at the wall, and the particle detachment rate to be proportional to σ,

$$\frac{\partial \sigma}{\partial t} = k_{\text{a}} c|_{\text{boundary}} - k_{\text{d}}\sigma. \tag{5}$$

The particle adhesion and detachment rate coefficients, k_{a} and k_{d}, are functions of the particle radius, the shear rate at the wall, as well as the surface chemistry of the particle and vessel walls. In Ref. [10], it is shown that the particle adhesion coefficient k_{a} is a decreasing function of particle size and shear rate and that the particle detachment coefficient k_{d} is highest for large particles and high shear rates.

3. The magnetic field and force

The force $\mathbf{F}_{\text{mag}}$ and torque $\mathbf{T}_{\text{mag}}$ on a particle in a magnetic field $\mathbf{B}(\mathbf{x})$ are described by the formulae $\mathbf{F}_{\text{mag}} = (\mathbf{m} \cdot \nabla)\mathbf{B}$ and $\mathbf{T}_{\text{mag}} = \mathbf{m} \times \mathbf{B}$, respectively, where $\mathbf{m}$ is the magnetic moment of the particle. Particles containing cores of magnetite material over 30 nm in diameter generally have a permanent magnetic moment [11]. The torque $\mathbf{T}_{\text{mag}}$ causes such particles to rapidly align with the magnetic field so that the force $\mathbf{F}^{\text{m}}_{\text{mag}}$ on a permanently magnetised particle becomes

$$\mathbf{F}^{\text{m}}_{\text{mag}} = \frac{|\mathbf{m}|}{|\mathbf{B}|}(\mathbf{B} \cdot \nabla)\mathbf{B}. \tag{6}$$

However magnetite particles of diameter smaller than 30 nm are generally superparamagnetic [11]. In this case $\mathbf{m}$ depends on the local magnetic flux density $\mathbf{B}$ and it is common to use a Langevin function to relate $\mathbf{m}$ to $\mathbf{B}$ [3],

$$\mathbf{m} = \frac{m_{\text{sat}}\mathbf{B}}{|\mathbf{B}|}L(|\mathbf{B}|), \quad L(|\mathbf{B}|) = \coth(\varepsilon|\mathbf{B}|) - \frac{1}{\varepsilon|\mathbf{B}|},$$
$$\varepsilon = \frac{m_{\text{sat}}}{kT},$$

where m_{sat} is the saturation magnetisation of the magnetic particle. Thus the force on a superparamagnetic particle is $\mathbf{F}^{\text{s}}_{\text{mag}} = m_{\text{sat}}L(|\mathbf{B}|)|\mathbf{B}|^{-1}(\mathbf{B} \cdot \nabla)\mathbf{B}$. For sufficiently weak fields $L(|\mathbf{B}|)$ can be linearised and $\mathbf{F}^{\text{s}}_{\text{mag}}$ approximated by

$$\mathbf{F}^{\text{s}}_{\text{mag}} \approx (\varepsilon m_{\text{sat}}/3)(\mathbf{B} \cdot \nabla)\mathbf{B} = \varepsilon m_{\text{sat}}\nabla(|\mathbf{B}|^2)/6. \tag{7}$$

Magnetic field varies over a lengthscale determined by the magnet size, typically $O(10^{-2}$–10^{-1} m). Typical diameters of the blood vessels in which targeting takes place are much smaller than this and thus magnetic force across a vessel diameter is approximately constant.

4. Two-dimensional network models

Optimisation of the magnetic targeting of drugs to tumours requires an understanding of the behaviour of magnetically targeted delivery in networks of blood vessels. However the solution of the Navier–Stokes equations and the advection diffusion model (3)–(5) (for $\mathbf{v}_{\text{b}}(\mathbf{x})$ and $c(\mathbf{x},t)$) in a three-dimensional network is a formidable computational task. Here we shall limit ourselves to considering a simplified 2-D network model, with the goal of obtaining a qualitative understanding of the targeting process.

4.1. Analysis of magnetic targeting in a single vessel

We start the network analysis by considering a 2-D model of a single small vessel, as shown in Fig. 1. The vessel has width $2d$ and length L. We

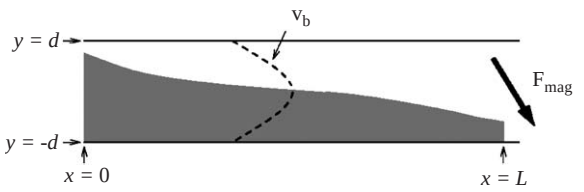

Fig. 1. The 2-D pipe geometry.

do not consider capillaries, for which the motion of individual blood cells must be studied. The blood velocity profile is assumed to be Poiseuille flow with mean velocity U_b, given by $\mathbf{v}_b(y) = 3/2U_b(1-y^2/d^2)\hat{\mathbf{x}}$ with corresponding shear rate $\dot{\gamma} = 3U_b|y|/d^2$. The true velocity profiles may be slightly blunted by the presence of blood cells, but this is not expected to be a significant effect [12]. Particles enter the tube at $x = 0$.

Here we write $\mathbf{F}_{mag} = \mathbf{F}_{mag}\hat{\mathbf{f}}$, where $|\hat{\mathbf{f}}| = 1$. We nondimensionalise (1)–(3) by scaling x with the vessel length L, y with the vessel half-width d, c with the inlet concentration c_{in} and t with the average time taken for a particle to pass through the vessel,

$$x = Lx', \quad y = dy', \quad t = \frac{L}{U_b}t',$$
$$c = c_{in}c', \quad \mathbf{v}_p = U_p\mathbf{v}'_p.$$

We now drop the primes from the notation, and work only with the nondimensional variables. The dimensionless version of Eq. (3) is

$$\frac{\partial c}{\partial t} + \frac{3}{2}(1-y^2)\frac{\partial c}{\partial x} + \frac{\partial}{\partial x}((\alpha\hat{\mathbf{f}}\cdot\hat{\mathbf{x}})c) + \frac{\partial}{\partial y}\left(\left(\frac{\alpha}{\delta}\hat{\mathbf{f}}\cdot\hat{\mathbf{y}}\right)c\right) = \frac{1}{Pe_{Br}}\left(\frac{\partial^2 c}{\partial x^2} + \frac{1}{\delta^2}\frac{\partial^2 c}{\partial y^2}\right) + \frac{1}{Pe_{sh}}\left(|y|\frac{\partial^2 c}{\partial x^2} + \frac{1}{\delta^2}\frac{\partial}{\partial y}\left(|y|\frac{\partial c}{\partial y}\right)\right) \quad (8)$$

for $|y|<1$, $0<x<1$. Here $Pe_{Br} = 6U_bL\pi\mu a/(kT)$ is the Brownian Peclet number and $Pe_{sh} = Ld/(3K_{sh}r_{RBC}^2)$ is the shear Peclet number, which give the ratio of the advective flux along the channel to the Brownian diffusive flux and shear-induced diffusive flux, respectively; $\delta = d/L$ is the aspect ratio of the vessel, and $\alpha = F_{mag}/(6\pi\mu a U_b)$ is the dimensionless magnetic velocity. The particle radius is denoted by the symbol a.

In Eq. (8), the term $(\alpha/\delta)(\partial c/\partial y)$ represents particle transport in a direction normal to the blood flow. Thus a significant fraction of the particles passing through the vessel will be trapped only if $\alpha/\delta \geqslant O(1)$. The value of α/δ is tabulated in Table 2 for particles of diameter 1.0×10^{-6}, 2.0×10^{-6}, 4.0×10^{-6} m containing 10% by volume magnetite in field gradients of $10\,T\,m^{-1}$ for four classes of blood vessel.

The terms $Pe_{Br}^{-1}\delta^{-2}(\partial^2 c/\partial y^2)$ and $Pe_{Sh}^{-1}\delta^{-2}(\partial^2 c/\partial y^2)$ in Eq. (8) give the diffusion of the magnetic particles across the flow streamlines. Using the parameters in Table 1, we find $Pe_{sh} \ll Pe_{Br}$ for all the particle diameters we consider (which implies shear-induced diffusion dominates Brownian diffusion). Shear-induced diffusion plays an important role in the transport and deposition of particles where the diffusive flux is strong enough to balance the advective flux due to the magnetic field. This is quantified by the dimensionless

Table 2
Estimates of $\alpha\delta^{-1}$, $Pe_{sh}^{-1}\delta^{-2}$ and $S = \alpha\delta Pe_{sh}$ for particles with diameter 1.0×10^{-6}, 2.0×10^{-6} and 4.0×10^{-6} m

Particle diameter, $2a$ (m)	Vessel type	$\alpha\delta^{-1}$	$Pe_{sh}^{-1}\delta^{-2}$	S
1×10^{-6}	Artery	1.6×10^{-3}	8.7×10^{-6}	1.8×10^{2}
1×10^{-6}	Arteriole	1.6×10^{-1}	1.2×10^{1}	1.3×10^{-2}
1×10^{-6}	Venule	1.2×10^{-1}	7.4×10^{-1}	1.6×10^{-1}
1×10^{-6}	Vein	9.4×10^{-4}	1.9×10^{-6}	5.0×10^{2}
2×10^{-6}	Artery	6.3×10^{-3}	8.7×10^{-6}	7.2×10^{2}
2×10^{-6}	Arteriole	6.3×10^{-1}	1.2×10^{1}	5.1×10^{-2}
2×10^{-6}	Venule	4.7×10^{-1}	7.4×10^{-1}	6.4×10^{-1}
2×10^{-6}	Vein	3.8×10^{-3}	1.9×10^{-6}	2.0×10^{3}
4×10^{-6}	Artery	2.5×10^{-2}	8.7×10^{-6}	2.9×10^{3}
4×10^{-6}	Arteriole	2.5×10^{0}	1.2×10^{1}	2.0×10^{-1}
4×10^{-6}	Venule	1.9×10^{0}	7.4×10^{-1}	2.6×10^{0}
4×10^{-6}	Vein	1.5×10^{-2}	1.9×10^{-6}	8.0×10^{3}

We used the value of $\mu = 3\times10^{-3}\,N\,s\,m^{-2}$ for the viscosity of blood. Typical saturation values of the mass magnetisation for magnetite particles are approximately $M_{sat} = 50\,A\,m^2\,kg^{-1}$ ($1\,A\,m^2\,kg^{-1} \equiv 1\,emu\,g^{-1}$). The density of magnetite is $5.1\times10^3\,kg\,m^{-3}$. We assume the magnetic field gradient is $\approx 10\,T\,m^{-1}$ at the target and that the particles contain 10% magnetite by volume ($\approx$33% by weight). The blood vessels dimensions are displayed in Table 1.

parameter S, which expresses the ratio of the advective and diffusive flux across the channel,

$$S = \alpha\delta Pe_{\mathrm{sh}} = \frac{F_{\mathrm{mag}} d^2}{16\pi\mu a U_{\mathrm{b}} K_{\mathrm{sh}} r_{\mathrm{RBC}}^2}. \tag{9}$$

The shear-induced diffusive flux must be included in the model if $S \leqslant \mathrm{O}(1)$, and in particular if $S \ll 1$ the particle flux due to the magnetic force is negligible in comparison to the flux due to shear-induced diffusion. Using the estimates shown in Table 2, we conclude that shear-induced diffusion can be an important effect within the arterioles and venules. Future work will examine the influence of the capture condition (5) on the deposition rate.

4.2. Two-dimensional network analysis at low Reynolds number, with $S \gg 1$, $\boldsymbol{\alpha}/\boldsymbol{\delta} = \mathrm{O}(1)$

Here we consider a simplified model of drug deposition in a network of vessels in the zero diffusion limit, $S \to \infty$. In addition transient effects are ignored and we look for steady-state solutions.

A common approach to determining $\mathbf{v}_{\mathrm{b}}$ in a complex network geometry is to approximate the network by a series of linear flow resistors connecting a set of junction nodes [13]. The relationship between the pressure drop $(p_i - p_j)$ between junctions nodes i and j and the flux Q_{ij} of blood in the vessel connecting i and j is calculated assuming a Poiseuille flow profile in each vessel,

$$Q_{ij} = w_{ij}(p_i - p_j), \quad w_{ij} = \frac{2d_{ij}^3}{3\mu L_{ij}},$$

where $2d_{ij}$ and L_{ij} are the width and length of the vessel joining nodes i and j. A sample network is shown in Fig. 2. The network flow is then determined by solving a system of sparse linear equations which enforce the conservation of mass at each junction, and specify the inlet/outlet pressures at each node on the boundary of the network,

$$\sum_j w_{ij}(p_i - p_j) = 0 \text{ for each junction}$$

$$p_i = p_i^{\mathrm{in}} \text{ for boundary nodes.}$$

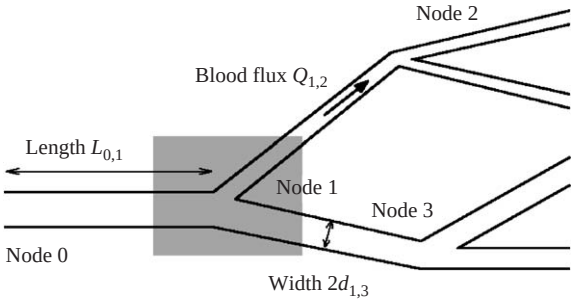

Fig. 2. An example of the network, showing node numbers and sample data values for d_{ij}, L_{ij} and Q_{ij}. The shaded area centred on node 1 is reproduced in Fig. 3.

This model is simple to solve, even for networks containing a large number of vessels. At low Reynolds numbers, such as those found in the microcirculation, the flow deviates from the Poiseuille flow only in a small region about the junction (labelled 'Junction region' in Fig. 3).

To complete the network model, we couple the flow model with the magnetic particle model (8) in the zero diffusion limit, $S \to \infty$. In this limit the governing partial differential equation changes type, from parabolic to hyperbolic, and so no boundary conditions are given except where the particle velocity is directed into the vessel, through the vessel wall; that is to say $c = 0$ where $\mathbf{v}_{\mathrm{p}} \cdot \mathbf{n} < 0$.

The concentration at any point in the vessel is either 0, or the initial inlet value, c_{in}. This is because we are considering the zero diffusion limit and $\mathbf{v}_{\mathrm{p}}$ is divergence free. The particle flux per unit length onto the vessel wall is $c_{\mathrm{in}}\mathbf{v}_{\mathrm{mag}} \cdot \mathbf{n}$. The flux of particles onto the vessel wall is computed by integrating this quantity along the vessel, however the total deposition rate cannot exceed the inlet flux, q_{ij}^{in}, thus

$$q_{ij}^{\mathrm{deposited}} = \min\left(\int_0^{L_{ij}} c_{\mathrm{in}}\mathbf{v}_{\mathrm{mag}} \cdot \mathbf{n}_{ij}\, \mathrm{d}l,\ \ q_{ij}^{\mathrm{in}} \right),$$

where $\mathbf{n}_{ij}$ is the outward normal to the wall (on which deposition occurs) of the vessel connecting nodes i and j. The inlet and outlet particle fluxes, q_{ij}^{in} and q_{ij}^{out}, therefore satisfy a simple conservation relation,

$$q_{ij}^{\mathrm{out}} = q_{ij}^{\mathrm{in}} - q_{ij}^{\mathrm{deposited}}.$$

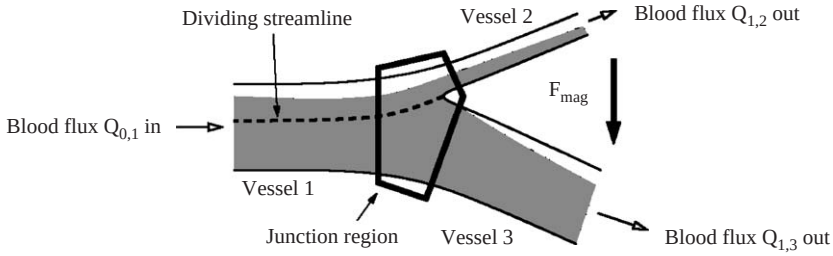

Fig. 3. An example of the division of the particles at a vessel junction with low Reynolds number flow conditions. The shaded regions of the pipes contain magnetic particles. This diagram corresponds to the highlighted region in Fig. 2.

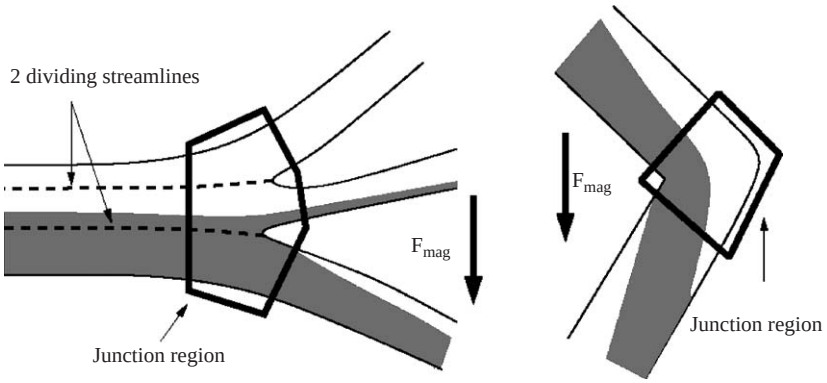

Fig. 4. The simple rules for determining the particle fluxes q_{ij} may be extended to cope with trifurcations and bends where deposition can occur on both vessel walls.

The division of particle flux at a simple vessel bifurcation is illustrated in Fig. 3. We can ignore the small amount of particle deposition which occurs inside the junction region and the effect of $\mathbf{v}_{\mathrm{mag}}$ in this small region since, at low Reynolds numbers, the junction region is very short compared to the length of the network vessels, L_{ij}. We consider the dividing streamline, which separates the fluid which passes into the two daughter vessels. Its position at the entrance to the junction region may be computed in a simple manner from the blood fluxes $Q_{0,1}$ (flowing between nodes 0 and 1), $Q_{1,2}$ (flowing between nodes 1 and 2) and the flux $Q_{1,3}$ (flowing between nodes 1 and 3). Using the Poiseuille flow profile in a channel of width $2d_{0,1}$, carrying a flux $Q_{0,1}$, the position of the dividing streamline is calculated by choosing the flux of blood above it equal to $Q_{1,2}$. The region of fluid containing particles at the outlet of the vessel connecting nodes 0 and 1 is computed from $q_{0,1}^{\mathrm{out}}$. Particles entering the junction region above the dividing streamline are assumed to enter the vessel connecting nodes 1 and 2, and particle below it are assumed to enter the vessel connecting nodes 1 and 3. We can thus compute the particle distribution without calculating the exact blood velocity field at each junction.

Other vessel junction topologies, such as converging flow at a junction, or trifurcations can lead to more complex distributions of the magnetic particles as shown in Fig. 4. These situations may be described using straightforward generalisations of the above technique. The network flow and particle deposition models were solved using Matlab.

Blood flow and particle deposition results obtained from the network model are shown in Fig. 5. This example shows a branching tree network; all the blood vessels have identical width and length. A uniform magnetic force

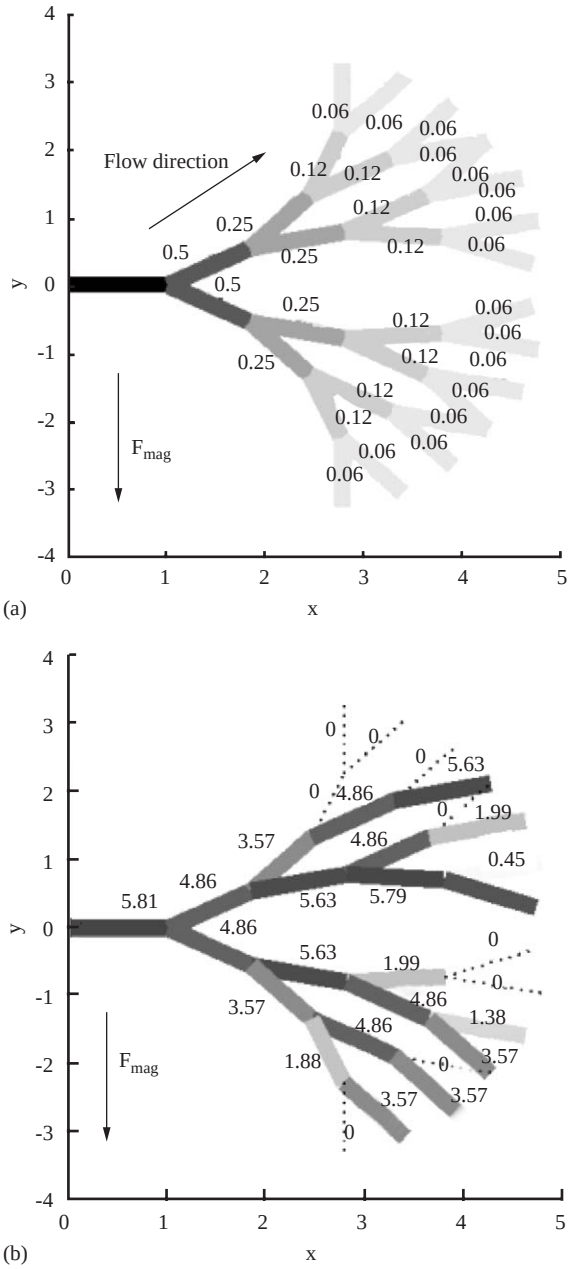

Fig. 5. (a) The division of blood flow in a simple branching tree model network of uniform vessels. The numbers and grey-scale shading indicate the fraction of flow in each vessel. (b) The numbers and grey-scale shading indicate the number of particles deposited in each vessel, as a percentage of the total flux of particles into the system. Overall, about 89% of the particles are captured in this model network. The magnetic force is assumed to be uniform in this example.

$\mathbf{F}_{\text{mag}} = -\mathbf{F}_{\text{mag}}\hat{\mathbf{y}}$ is applied to the particles. Blood and magnetic particles enter the network through a single vessel at $(x, y) = (0, 0)$. The blood flows through the branches of the tree network to the terminal nodes, where a uniform fluid pressure, $p = 0$, is prescribed. The division of the blood flow between the branches of the network is shown in Fig. 5(a). The flow is distributed evenly over the vessels at each level of the network. Fig. 5(b) shows the number of magnetic particles captured in each vessel, as a percentage of the total number of particles entering the network. Overall, about 89% of the particles are trapped in this example, and 11% are washed out of the network through the terminal vessels. Despite the even distribution of blood flow in the network the particle distribution is quite heterogeneous, with no particles being trapped in some vessels. The deposition pattern depends strongly on the alignment of the vessels with respect to the force $\mathbf{F}_{\text{mag}}$. Although a large number of particles are trapped in the first vessel, this represents only a small fraction of the total number of particles flowing through this vessel. In contrast, the number of particles captured in the fourth and fifth generation vessels is small, but this constitutes a large fraction of the particles entering these vessels. This is consistent with the observation that the efficiency of magnetic particle capture depends on the parameter ratio α/δ.

7. Designing the magnetic field

It is clear from the preceding discussion that increasing particle uptake onto the vessel walls within a target region can be achieved by increasing the magnetic force experienced by the particles in that region. Ideally we would like to obtain a maximum of the magnetic force in the target region. However, as we shall demonstrate in two-dimensions, this is only possible (using an externally applied magnetic field) if the target region lies on the surface of the body. We now set out to demonstrate the following statement:

Statement: If the magnetic field is applied externally to the body then there can be no point within the body where the magnitude of the force on a (superparamagnetic or permanently

magnetised) particle takes a maximum value. This statement is only proved for a 2-D magnetic field (although we suspect it to be true in three-dimensions).

External to the magnet the magnetic field may be expressed in terms of a scalar potential, $\mathbf{B} = \nabla\phi$ (since permeability is approximately constant and no significant currents flow in the region external to the magnet). Furthermore since $\mathbf{B}$ is divergence free we have $\nabla \cdot \mathbf{B} = \nabla^2\phi = 0$. It follows that the forces on a superparamagnetic particle $\mathbf{F}^{\mathrm{s}}_{\mathrm{mag}}$ (in a weak field) and a permanently magnetised particle $\mathbf{F}^{\mathrm{m}}_{\mathrm{mag}}$ are, from Eqs. (6)–(7),

$$\mathbf{F}^{\mathrm{s}}_{\mathrm{mag}} = \frac{\varepsilon m_{\mathrm{sat}}}{6}\nabla(|\nabla\phi|^2),$$

$$\mathbf{F}^{\mathrm{m}}_{\mathrm{mag}} = \frac{|\mathbf{m}|}{2|\nabla\phi|}\nabla(|\nabla\phi|^2) = |\mathbf{m}|\nabla(|\nabla\phi|).$$

Proof of the Statement. The magnitude of the force $\mathbf{F}^{\mathrm{s}}_{\mathrm{mag}}$ on a superparamagnetic particle takes a maximum where $|\nabla(|\nabla\phi|^2)|^2$ has a maximum. In the case where the magnetic field is 2-D (i.e. $\mathbf{B} = \mathbf{B}(x, y)$), we can write

$$|\nabla(|\nabla\phi(x,y)|^2)|^2 = \alpha_x^2 + \alpha_y^2, \quad \text{where} \quad \alpha = \phi_x^2 - \phi_y^2,$$

by noting that $\phi_{xx} = -\phi_{yy}$. It is straightforward to show that if $\nabla^2\phi = 0$ then $\nabla^2\alpha = 0$. Now for a maximum of magnetic force we require $\alpha_x^2 + \alpha_y^2$ to take a maximum. Without loss of generality we can orientate the coordinate system such that at the maximum, $\alpha_y = 0$. This implies that α_x^2 has a local maximum, and hence α_x has a local maximum or minimum, at this point. However α_x satisfies Laplace equation $\nabla^2(\alpha_x) = 0$, since α does, and thus by the maximum principle [14], α_x cannot have an interior local maximum or an interior local minimum (here interior means wholly within the region in which $\nabla^2\phi = 0$; i.e. away from the magnet). Thus $\alpha_x^2 + \alpha_y^2$ cannot have an internal maximum. Hence that the magnetic force on a paramagnetic particle has no maxima internal to the body (they occur on the magnet).

The magnitude of the force $\mathbf{F}^{\mathrm{m}}_{\mathrm{mag}}$ on a permanently magnetised particle takes a maximum where $|\nabla(|\nabla\phi|^2)|^2/|\nabla\phi|^2$ has a maximum. Where the magnetic field is 2-D we can write

$$\frac{|\nabla(|\nabla\phi(x,y)|^2)|^2}{|\nabla\phi(x,y)|^2} = \alpha_x^2 + \alpha_y^2, \quad \text{where} \quad \alpha = 2\phi_x.$$

Again it is clear that $\nabla^2\alpha = 0$ and hence that $\alpha_x^2 + \alpha_y^2$ cannot have an internal maximum by a similar argument to that given above.

The fact that the magnetic force on a particle cannot take a maximum magnitude within the body (away from the source of the magnetic field) means that, where the drug/particle complex is injected systemically, it is impossible to target regions deep within the body without targeting some surrounding regions more strongly.

8. Conclusion

We have formulated a model of magnetic particle transport in the intermediate sized vessels of the blood stream which incorporates the effects of shear-induced diffusion (which arises as a result of interactions between red blood cells). The model depends crucially on the dimensionless parameter S, (see Eq. (9)). In particular if $S \ll 1$ the effects of the magnetic force are negligible in comparison to those of shear-induced diffusion. Estimates for magnetic particles of diameter 1×10^{-6}–4×10^{-6} m containing magnetite nanoparticles (10% by volume) confirm that the diffusive flux may significantly disrupt particle deposition in arterioles and venules. The effects of magnetic targeting in the capillaries have yet to be modelled.

We have demonstrated a simple network model which can describe the deposition of magnetic particles in a hierarchy of vessels and observed that the orientation of the vessels with respect to the magnetic force crucially affects particle depositions rates leading to heterogeneous particle distributions. In addition we have shown (in a 2-D analysis) that it is not possible to obtain a maximum of magnetic force (on a magnetic particle) inside the body, using an externally applied magnetic field. Since drug targeting is effected by pulling magnetic particles to the edge of vessels this suggests that it will not be possible

to target interior regions of the body without targeting some of the surrounding regions of the body more strongly. Furthermore we do not expect magnetic traps to be of use in this application since magnetic particles are constrained to move around the body in linear vessels and the magnitude of magnetic field required to hold a particle in the main flow, of all but the very smallest of vessels, is very large. This leads us to conjecture that the use of magnetically targeted drug delivery with an externally applied field is appropriate only for targets close to the surface of the body.

Acknowledgements

We wish to thank the EPSRC (Grant GR/R 94176) for funding this work and Prof. J.R. King and Prof. J. Dobson for helpful discussions.

References

[1] S. Goodwin, et al., J. Magn. Magn. Mater. 194 (1999) 132.
[2] A.S. Lübbe, C. Alexiou, C. Bergemann, J. Surg. Res. 95 (2001) 200.
[3] C.F. Driscoll, et al., Microvasc. Res. 27 (1984) 353.
[4] G. Richardson, et al., Report of the First Mathematical Medicine Study Group, Nottingham, 2000.
[5] A.J. Goldman, R.G. Cox, H. Brenner, Chem. Eng. Sci. 22 (1967) 653.
[6] H.L. Goldsmith, Fed. Proc. 30 (1971) 1578.
[7] N.-H.L. Wang, K.H. Keller, J. Colloid Interface Sci. 103 (1985) 210.
[8] A.L. Zydney, C.K. Colton, PhysicoChem. Hydrodyn. 10 (1988) 77.
[9] R.B. Bird, W.E. Stewart, Transport Phenomena, Wiley, New York, 1960.
[10] V.R. Shinde Patil, et al., Biophys. J. 80 (2001) 1733.
[11] Q.A. Pankhurst, et al., J. Phys. D 36 (2003) R167.
[12] C.G. Caro, et al., The Mechanics of the Circulation, Oxford University Press, Oxford, 1978.
[13] D.A. Beard, J.B. Bassingthwaighte, Ann. Biomed. Eng. 28 (2000) 253.
[14] J.R. Ockendon, et al., Applied Partial Differential Equations, Oxford University Press, Oxford, 1999.